Supplementary Information

Structural insights into the LGR4-RSPO2-ZNRF3 complexes regulating WNT/β-catenin signaling

Lu Wang[1,†], Fangzheng Hu[1,†], Qianqian Cui[1,†], Huarui Qiao[1,†], Lingyun Li[1,†], Tengjie Geng[1,†], Yuying Li[1,†], Zengchao Sun[1], Siyu Zhou[1], Zhongyun Lan[1], Shaojue Guo[1], Ying Hu[3], Jiqiu Wang[4,5], Qilun Yang[6], Zenan Wang [3 *], Yuanyuan Dai[7,8, *], Yong Geng[1,2, *]

[1] State Key Laboratory of Drug Research, Shanghai Institute of Materia Medica, Chinese Academy of Sciences, Shanghai, 201203, China.

[2] University of Chinese Academy of Sciences, Beijing, 100049, China.

[3] Center for Cognitive Technology, Shenzhen Institute of Advanced Technology, Chinese Academy of Sciences, Shenzhen, Guangdong, 518055, China.

[4]Department of Endocrine and Metabolic Diseases, Shanghai Institute of Endocrine and Metabolic Diseases, Ruijin Hospital, Shanghai Jiao Tong University School of Medicine, Shanghai, 200025, China.

[5]Shanghai National Clinical Research Center for Metabolic Diseases, Key Laboratory for Endocrine and Metabolic Diseases of the National Health Commission of the PR China, Shanghai National Center for Translational Medicine, Shanghai, 200025, China.

[6]Shanghai Kailuo Biotechnology Co., Ltd, Shanghai, 201600, China.

[7]Department of Pharmacy, National Cancer Center/National Clinical Research Center for Cancer/Cancer Hospital, Chinese Academy of Medical Sciences and Peking Union Medical College, Beijing, 100021, China.

[8] National Cancer Center/National Clinical Research Center for Cancer/Cancer Hospital of Chinese Academy of Medical Sciences, Langfang Campus, Langfang, 065001, China

[†]These authors contributed equally: Lu Wang, Fangzheng Hu, Qianqian Cui, Huarui Qiao, Lingyun Li, Tengjie Geng, and Yuying Li.

* Correspondence: gengyong@simm.ac.cn, daiyuanyuan@cicams.ac.cn, zn.wang1@siat.ac.cn.

Supplementary Fig. 1 | Generation and characterization of camelid nanobody.

Supplementary Fig. 2 | Cryo-EM data analysis of the LGR4-RSPO2-ZNRF3(RING)-MB52 complex (1:1:1, heterotrimer).

Supplementary Fig. 3 | Cryo-EM data analysis of the LGR4-RSPO2-ZNRF3(RING)-MB52 complex (1:2:2, pentamer B).

Supplementary Fig. 4 | Cryo-EM data analysis of the LGR4-RSPO2ZNRF3(ΔRING)-MB52 complex (2:2:2, di-heterotrimer and 1:2:2, pentamer A).

Supplementary Fig. 5 | The models of the heterotrimer, pentamer A, pentamer B, and di-heterotrimer.

Supplementary Fig. 6 | Superposition of the map and model of the LGR4-RSPO2-ZNRF3.

Supplementary Fig. 7 | Flow cytometric analysis of cell surface expression levels.

Supplementary Fig. 8 | RSPO2 cannot activate LGR4.

Supplementary Fig. 9 | Side-by-side comparation of LGR4 conformation in different complexes.

Supplementary Fig. 10 | TM Domain Sequence Alignment of LGR4 with LGR5 and RNF43 with ZNRF3, with Structural Comparison of ZNRF3 and RNF43.

Supplementary Table. 1 | Cryo-EM data collection, refinement, and validation statistics.

Supplementary Table. 2 | Oligonucleotide primers/gene fragments used in this study**.**

Supplementary Table. 3 | FACS sequential gating in this study.

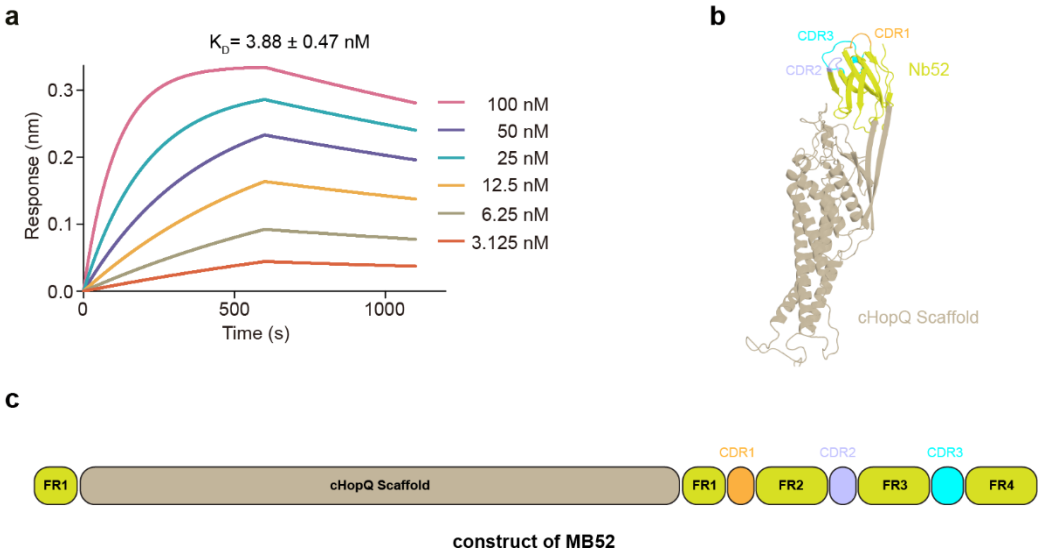

Supplementary Fig. 1 | Generation and characterization of camelid nanobody.

a, Measurement of binding affinity between NB52 and LGR4 using biolayer interferometry (BLI) and fitting with a 1:1 binding model. **b**, the model of MB52 predicted by the Swiss model. **c**, Domain compositions of MB52 are indicated schematically.

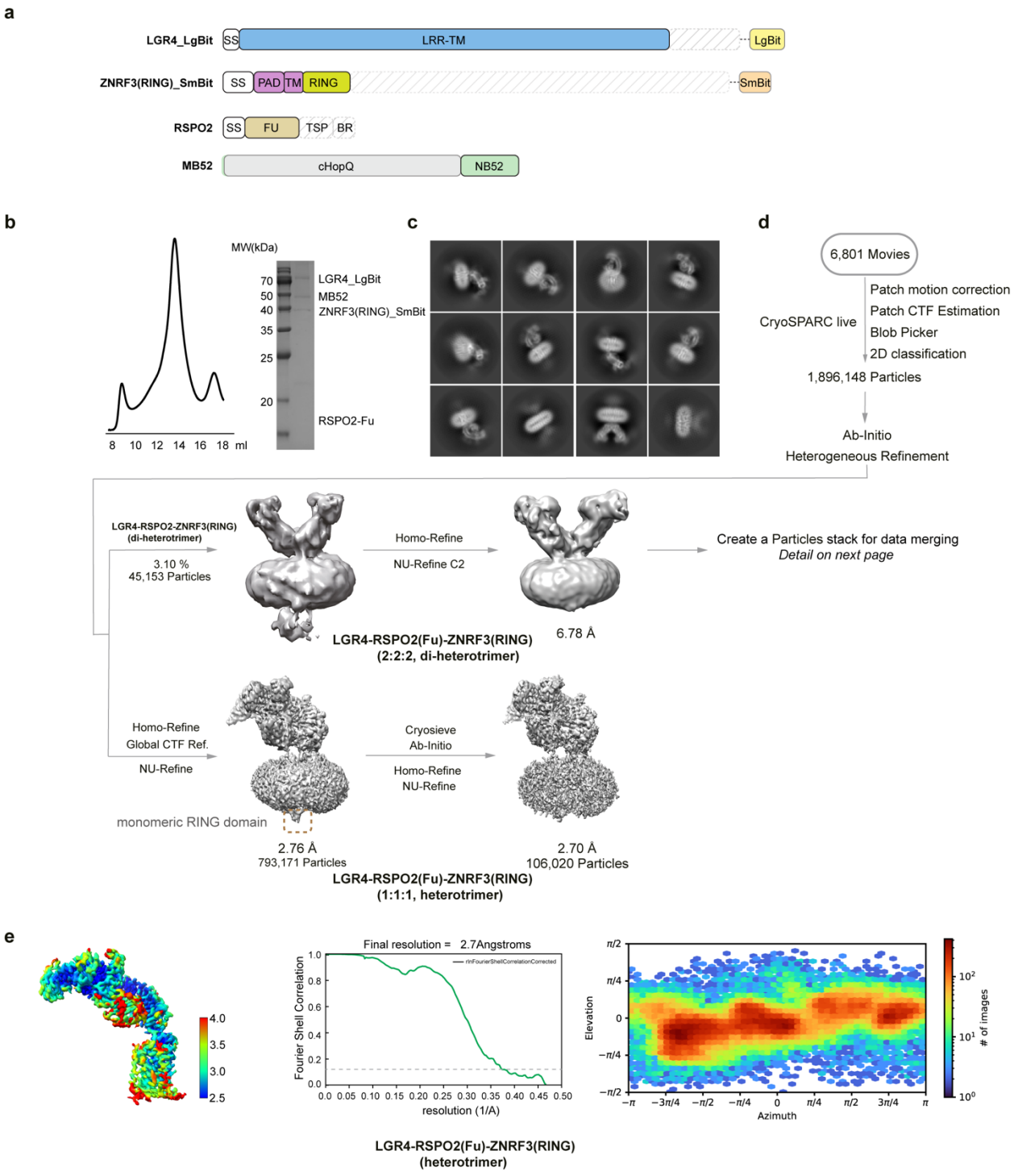

Supplementary Fig. 2 | Cryo-EM data analysis of the LGR4-RSPO2-ZNRF3(RING)-MB52 complex (1:1:1, heterotrimer). a, Domain compositions of LGR4, ZNRF3, RSPO2, and MB52 are indicated schematically, along with a schematic representation of their constructs used for structure determination. **b**, SEC profiles (left) and SDS-PAGE (right) of the LGR4-RSPO2(Fu)-ZNRF3(RING)-MB52 complex with a 1:1:1 stoichiometry

(heterotrimer,). Genetic fusions of LgBiT and HiBiT were introduced at the C-terminus of LGR4 and the ZNRF3 RING domain (including the RING domain), the band corresponding to LGR4 appears smeared due to high glycation. **c,** 2D classification of the particles for the LGR4-RSPO2-ZNRF3-MB52 complex. The particles encompass complexes in ratios of 1:1:1, and 2:2:2. **d**,**e** Flowchart illustrating the Cryo-EM image acquisition and data processing steps used to obtain the structure of the LGR4-RSPO2(Fu)-ZNRF3(RING)-MB52 complex (1:1:1, heterotrimer) (**d**), along with their corresponding local resolution and Fourier shell correlation (FSC) curves (**e**).

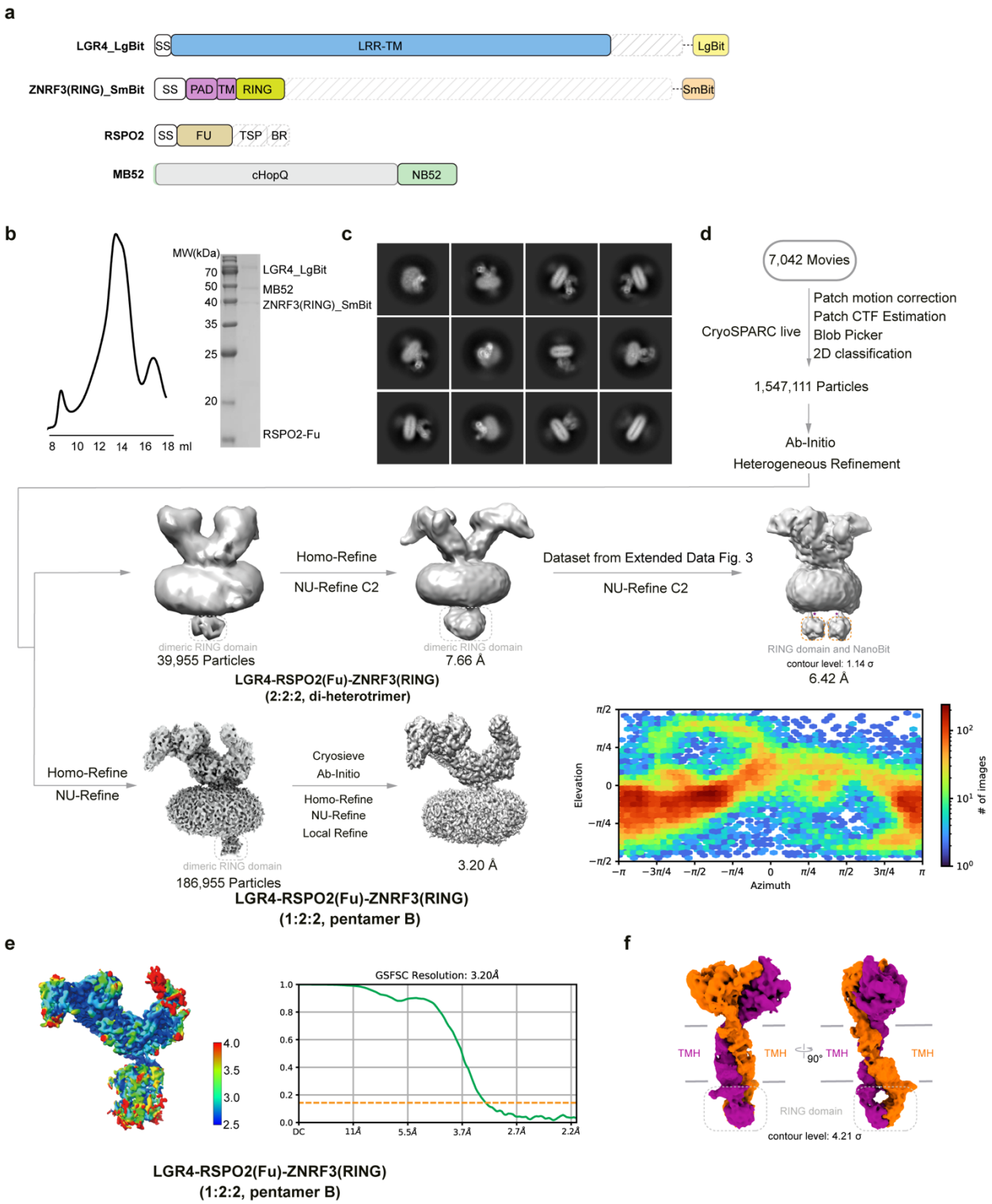

Supplementary Fig. 3 | Cryo-EM data analysis of the LGR4-RSPO2-ZNRF3(RING)-MB52 complex (1:2:2, pentamer B). a, Domain compositions of LGR4, ZNRF3, RSPO2, and MB52 are indicated schematically, along with a schematic representation of their constructs used for structure determination. **b**, SEC profiles (left) and SDS-PAGE (right) of the LGR4-

RSPO2(Fu)-ZNRF3(RING)-MB52 complex (1:2:2, pentamer B), Genetic fusions of LgBiT and HiBiT were attached to the C-terminus of LGR4 and the ZNFR3 RING domain (including the RING domain). The band corresponding to LGR4 appears smeared due to high glycation. **c,** 2D classification of the particles for the LGR4-RSPO2-ZNRF3(RING)-MB52 complex with a 1:2:2 ratio. **d**, Flowchart illustrating the Cryo-EM image acquisition and data processing steps used to obtain the structure of the LGR4-RSPO2-ZNRF3(RING)-MB52 complex (1:2:2, pentamer B), along with their corresponding local resolution and Fourier shell correlation (FSC) curves (**e**). **f**, Map of ZNRF3 in the pentamer B in low-pass-filtered map (contour level: 4.21σ).

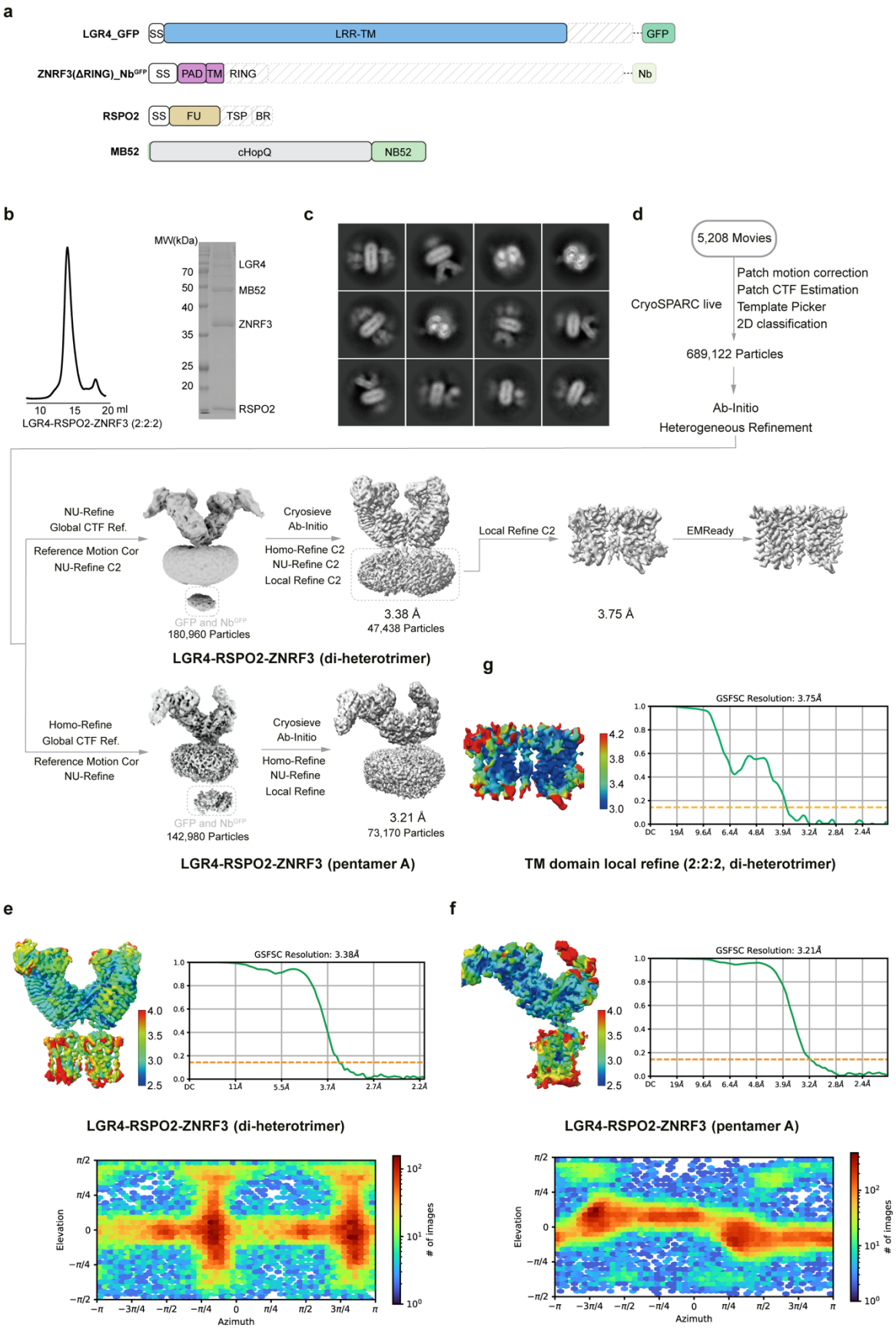
a
LGR4_GFP
SS
LRR-TM
GFP
ZNRF3(ΔRING)_Nb^GFP
SS
PAD
TM
RING
Nb
RSPO2
SS
FU
TSP
BR
MB52
cHopQ
NB52
b
MW(kDa)
70
50
40
35
25
20
LGR4
MB52
ZNRF3
RSPO2
10 15 20 ml
LGR4-RSPO2-ZNRF3 (2:2:2)
c
d
5,208 Movies
CryoSPARC live
Patch motion correction
Patch CTF Estimation
Template Picker
2D classification
689,122 Particles
Ab-Initio
Heterogeneous Refinement
NU-Refine
Global CTF Ref.
Reference Motion Cor
NU-Refine C2
GFP and Nb^GFP
180,960 Particles
Cryosieve
Ab-Initio
Homo-Refine C2
NU-Refine C2
Local Refine C2
3.38 Å
47,438 Particles
Local Refine C2
3.75 Å
EMReady
LGR4-RSPO2-ZNRF3 (di-heterotrimer)
Homo-Refine
Global CTF Ref.
Reference Motion Cor
NU-Refine
GFP and Nb^GFP
142,980 Particles
Cryosieve
Ab-Initio
Homo-Refine
NU-Refine
Local Refine
3.21 Å
73,170 Particles
LGR4-RSPO2-ZNRF3 (pentamer A)
g
GSFSC Resolution: 3.75Å
TM domain local refine (2:2:2, di-heterotrimer)
e
GSFSC Resolution: 3.38Å
LGR4-RSPO2-ZNRF3 (di-heterotrimer)
Elevation
Azimuth
# of images
f
GSFSC Resolution: 3.21Å
LGR4-RSPO2-ZNRF3 (pentamer A)
Elevation
Azimuth
# of images

Supplementary Fig. 4 | Cryo-EM data analysis of the LGR4-RSPO2ZNRF3(ΔRING)-MB52 complex (2:2:2, di-heterotrimer and 1:2:2, pentamer A). a, Domain compositions of LGR4, ZNRF3, RSPO2, and MB52 are indicated schematically, along with a schematic representation of their constructs used for structure determination. **b**, SEC profiles (left) and SDS-PAG (right) of the LGR4-RSPO2-ZNRF3(ΔRING)-MB52 complex (2:2:2, di-heterotrimer, and 1:2:2, pentamer A), In these complexes, GFP and anti-GFP nanobody were genetically fused to the C-terminus of LGR4 and ZNRF3ΔRING (RING domain truncated). The band corresponding to LGR4 appears smeared due to high glycation. **c,** 2D classification of the particles for the LGR4-RSPO2-ZNRF3(ΔRING)-MB52 complex (di-heterotrimer, with a 2:2:2 stoichiometry, and pentamer A, with a 1:2:2 stoichiometry). **d**, Flowchart illustrating the Cryo-EM image acquisition and data processing steps used to obtain the structure of the LGR4-RSPO2-ZNRF3(ΔRING)-MB52 complex (2:2:2**,** di-heterotrimer) and the LGR4-RSPO2-ZNRF3(ΔRING)-MB52 complex (1:2:2, pentamer A), along with their corresponding local resolution and Fourier shell correlation (FSC) curves (**e**-**g**).

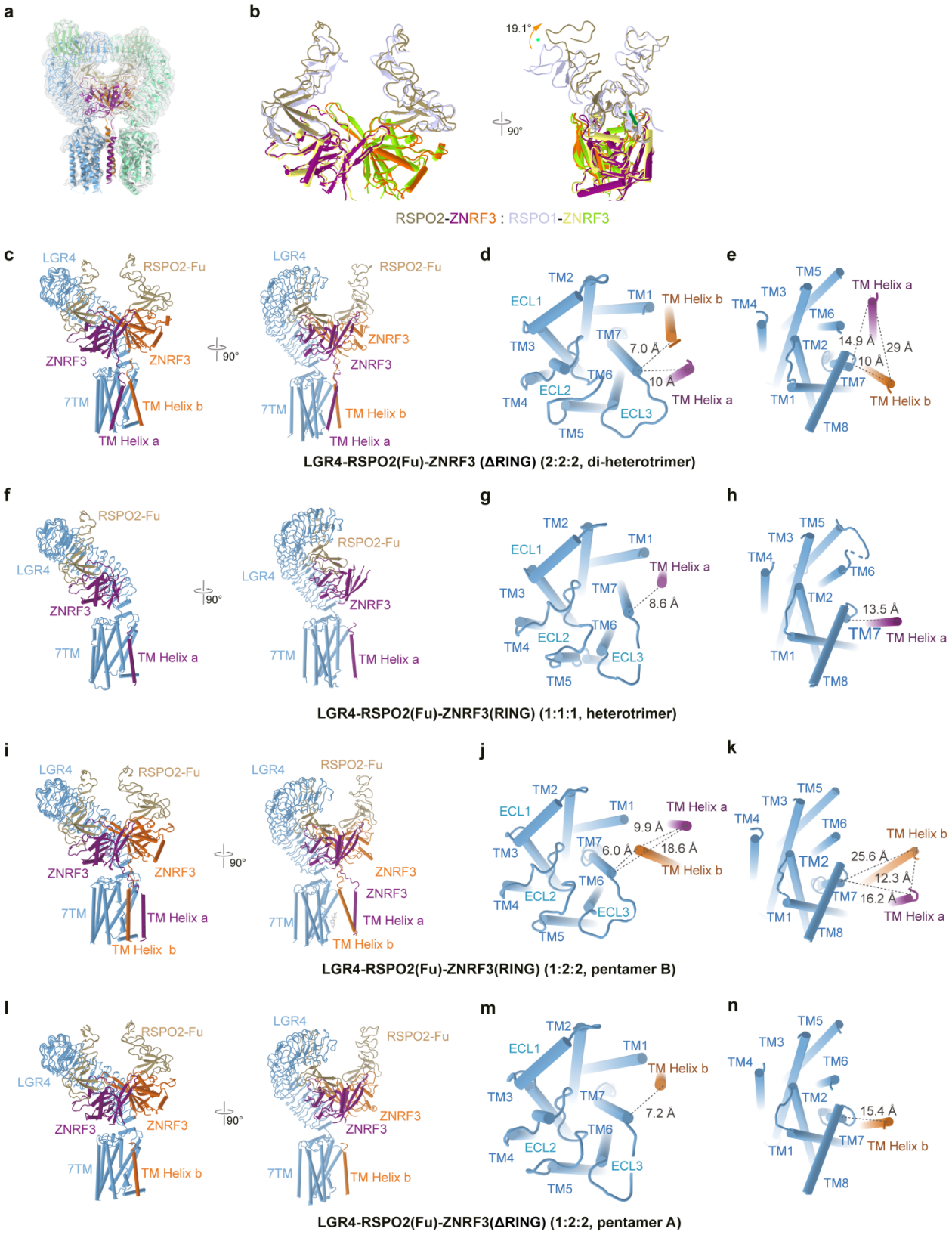

Supplementary Fig. 5 | The models of the heterotrimer, pentamer A, pentamer B, and di-heterotrimer. a, Superposition of map and model of the di-heterotrimer complex. **b**, Conformational comparison of RSPO2-ZNRF3 of LGR4-RSPO2-ZNRF3(ΔRING) complex

(2:2:2, di-heterotrimer) with previously report in the RSPO1-ZNRF3 (PDB: 4CDK, RMSD=0.901, 274 to 274 atoms). **c**, The models of the di-heterotrimer complex from two views (one LGR4 is omitted for clarity). **d**, **e**, The transmembrane region of the di-heterotrimer complex is shown from the top view (**d**) and bottom view (**e**). **f**, The models of the heterotrimer complex from two views. **g**, **h**, The transmembrane region of the heterotrimer complex is shown from the top view (**g**) and bottom view (**h**). **i**, The models of the pentamer B from two views. **j**, **k**, The transmembrane region of the pentamer B complex is shown from the top view (**j**) and bottom view (**k**). **l**, The models of the pentamer A from two views. **m**, **n**, The transmembrane region of the pentamer A complex is shown from the top view (**m**) and bottom view (**n**).

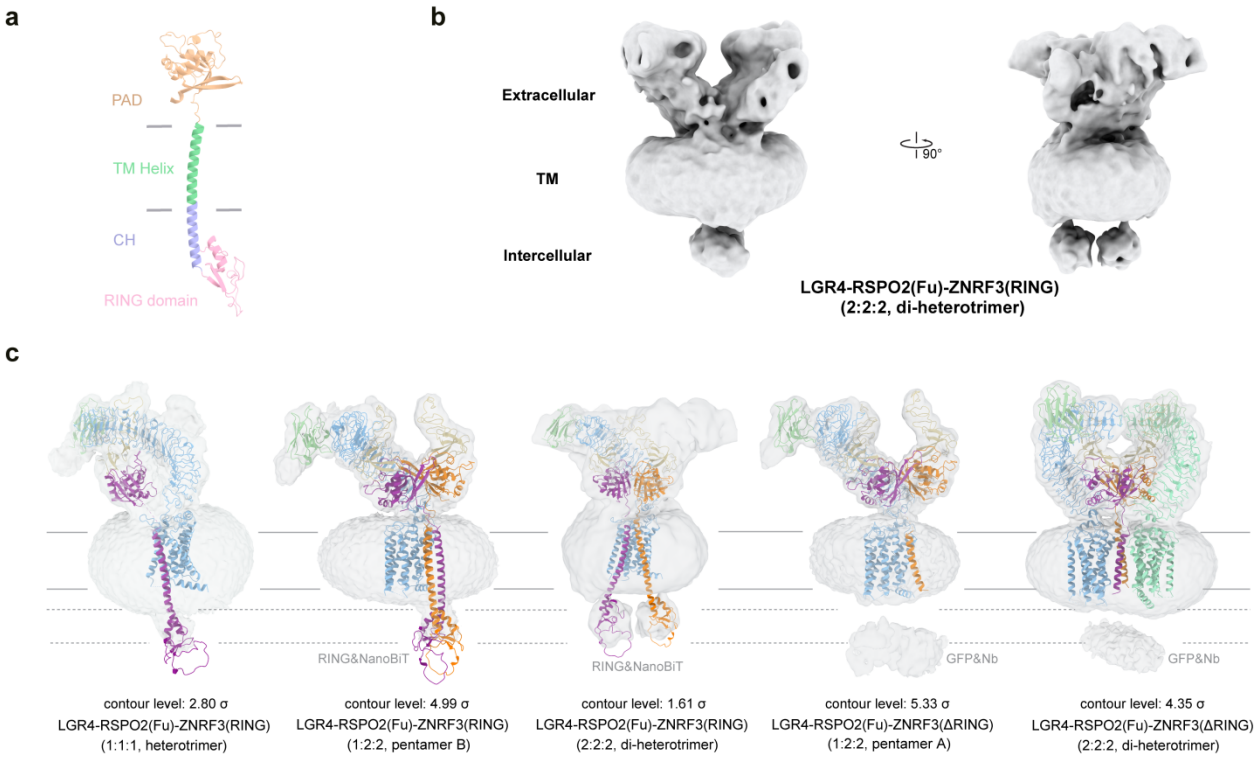

Supplementary Fig. 6 | Superposition of the map and model of the LGR4-RSPO2-ZNRF3.

a, The model of ZNRF3(ΔC-termini) is predicted by Swiss-model. **b**, The map of the LGR4-RSPO2-ZNRF3(RING) complex in its di-heterodimer form (2:2:2), with ZNRF3 containing the RING domain. **b**, Superposition of the map and model of the LGR4-RSPO2-ZNRF3 complexes.

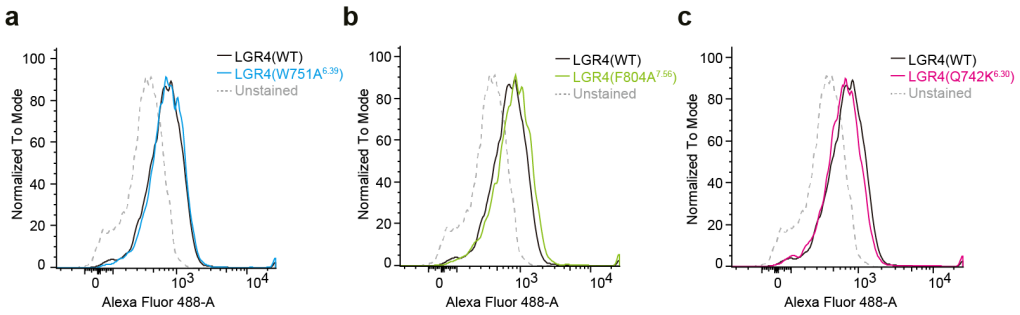

Supplementary Fig. 7 | Flow cytometric analysis of cell surface expression levels.

Flow cytometric analysis of cell surface expression levels shows that LGR4 mutants exhibit approximately 100% expression relative to the wild-type (WT) LGR4. HEK293T cells were transiently transfected with Flag-tagged WT LGR4 or the indicated mutants for 12 hours and subsequently treated with RSPO1. Cells were stained with an anti-Flag monoclonal antibody, followed by washing and incubation with Alexa Fluor® 488 Goat Anti-Mouse IgG. After further washing, samples were analyzed using a BD Fortessa™ flow cytometer, and data were processed with FlowJo Software (FlowJo, LLC). In the flow cytometry histograms, unstained cells are represented by dashed lines, while WT LGR4 is displayed in black. Mutants are color-coded as follows: W751A$^{6.39}$ in cyan (**a**), F804A$^{7.56}$ in green (**b**), and Q742K$^{6.30}$ in pink (**c**). The near-complete overlap of each mutant's histogram with WT indicates that the cell surface expression levels of the mutants are unaffected, demonstrating comparable expression to WT LGR4.

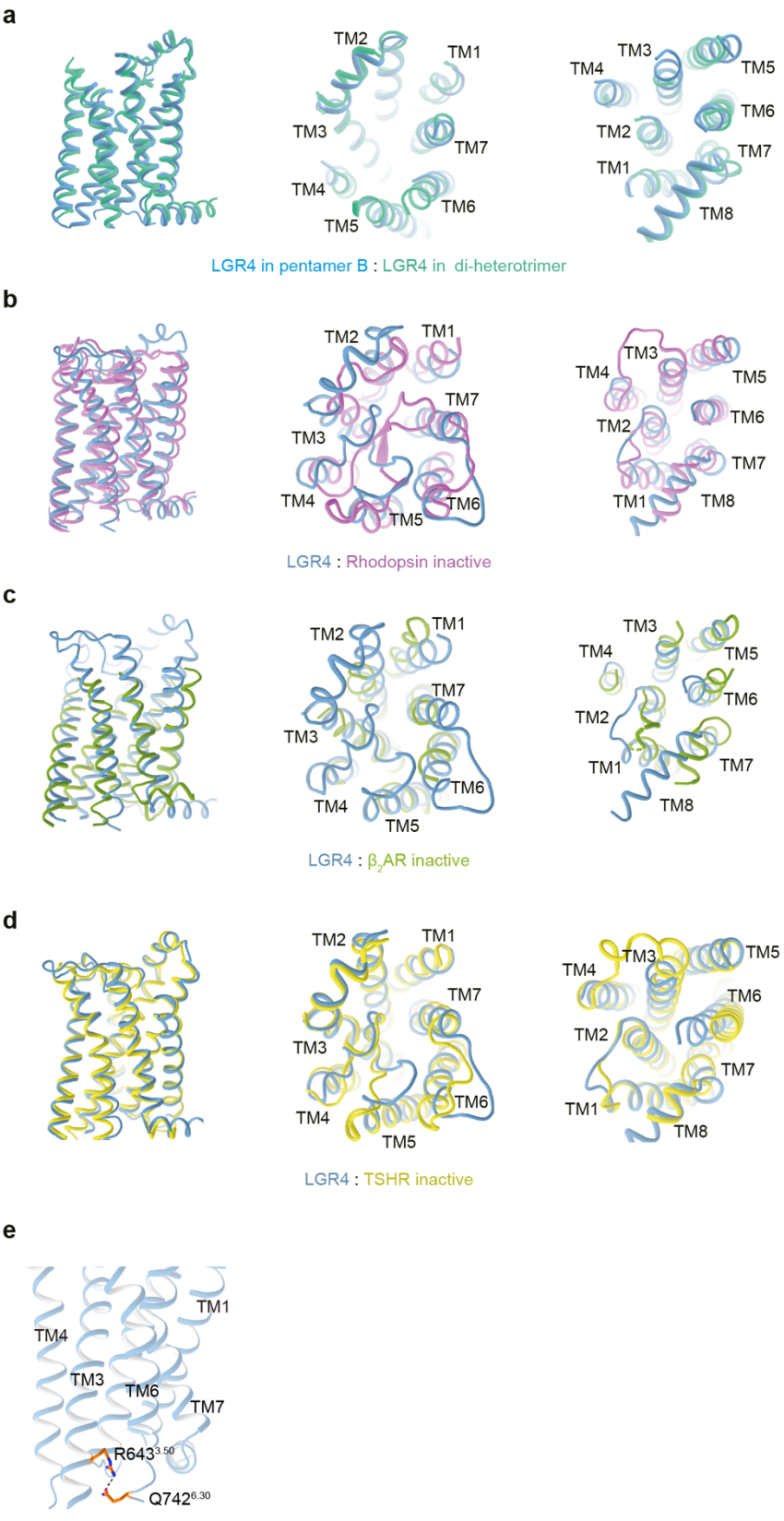

legend on next page

Supplementary Fig. 8 | RSPO2 cannot activate LGR4.

a, Conformational comparison of TMD of LGR4 in pentamer B (light blue) with that in the di-heterotrimer (greencyan) from the front view (left), top view (middle) and bottom view (right), RMSD =1.142 (260 to 260 atoms). **b**-**d**, Conformational comparison of TMD of LGR4 (light blue) with that in the inactive rhodopsin receptor (**b**, magenta, PDB:1GZM, RMSD=4.075, 190 to 190 atoms), β_2AR (**c**, light green, PDB:2R4S, RMSD=4.675, 114 to 114 atoms), TSHR (**d**, yellow, PDB:7XW7, RMSD=1.077, 174 to 174 atoms) from the front view (left), top view (middle) and bottom view (right). **e**, The ionic lock between R643$^{3.50}$ of TM3 and Q742$^{6.30}$ of TM6 in LGR4.

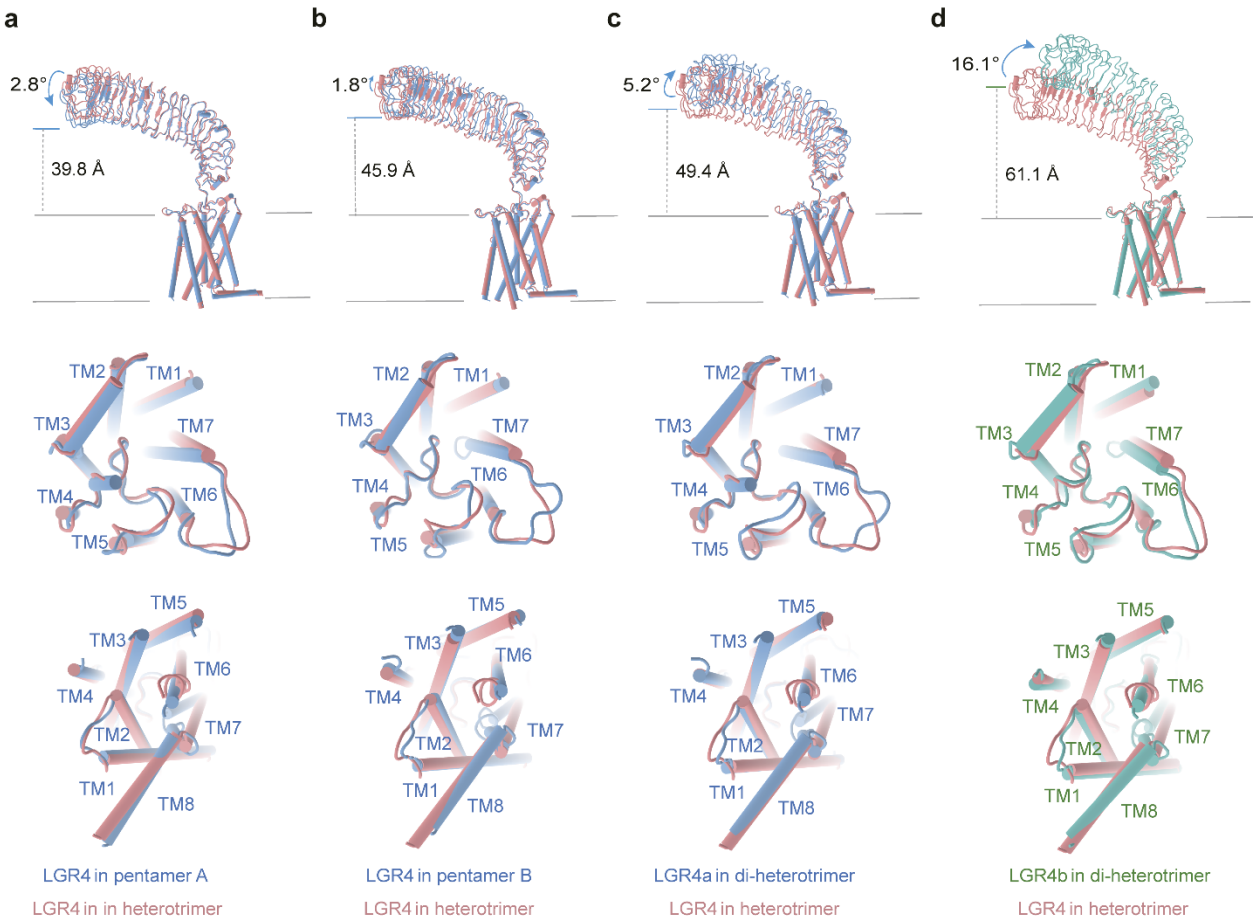

Supplementary Fig. 9 | Side-by-side comparation of LGR4 conformation in different complexes.

a-d, The superimposition of LGR4 (pink) in heterotrimer and that in different complexes: LGR4 in pentamer A (**a**, RMSD = 0.659 (174 to 174 atoms)), LGR4 in pentamer B (**b**, RMSD = 0.510 (174 to 174 atoms)), LGR4a in di-heterotrimer (**c**, RMSD = 0.842 (174 to 174 atoms)), and LGR4b in the heterotrimer (**d**, cyan, RMSD = 1.170 (174 to 174 atoms)). The first line shows the front view, while the second and third lines show the transmembrane domain from the top and bottom view. The rotation angle of the ECD of LGR4 in different complexes and the perpendicular distance from the G45 Cα of LGR4 to the membrane layer are indicated.

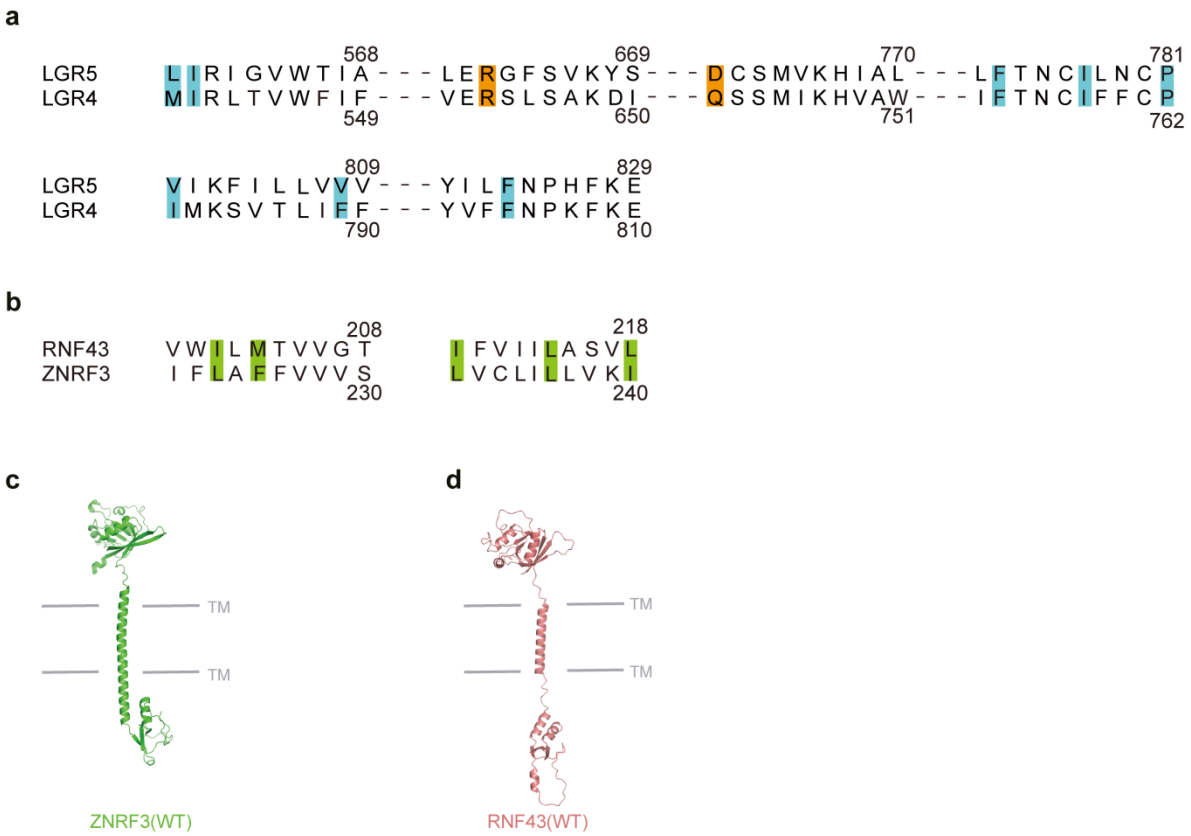

Supplementary Fig. 10 | TM Domain Sequence Alignment of LGR4 with LGR5 and RNF43 with ZNRF3, with Structural Comparison of ZNRF3 and RNF43.

a, Sequence alignment between LGR4 and LGR5. **b**, Sequence alignment between ZNRF3 and RNF43. Specific interaction residues within the transmembrane regions of LGR4 and ZNRF3 are highlighted: LGR4 residues are shown in light blue, and ZNRF3 residues in green. The ionic lock is indicated in orange. **c, d**, The AlphaFold-predicted structures of ZNRF3 (green)(c) and RNF43 (orange) (**d)**.

Supplementary Table. 1 | Cryo-EM data collection, refinement, and validation statistics.

	LGR4-RSPO2-ZNRF3(RING) (1:1:1, heterotrimer) (EMDB-38309) (PDB 8XFT)	LGR4-RSPO2-ZNRF3(ΔRING) (1:2:2, pentamer A) (EMDB-38307) (PDB 8XFP)	LGR4-RSPO2-ZNRF3(RING) (1:2:2, pentamer B) (EMDB-38308) (PDB 8XFS)	LGR4-RSPO2-ZNRF3(ΔRING) (2:2:2, di-heterotrimer) (EMDB-38982) (PDB 8Y69)
Data collection and processing				
Magnification	81,000	81,000	81,000	81,000
Voltage (kV)	300	300	300	300
Electron exposure (e–/Å^2)	70	70	70	70
Defocus range (μm)	-1.5 to -2.5	-1.5 to -2.5	-1.5 to -2.5	-1.5 to -2.5
Pixel size (Å)	0.5355	0.5355	0.5355	0.5355
Symmetry imposed	C1	C1	C1	C2
Initial particle images (no.)	2,481,288	2,559,524	1,892,487	2,559,524
Final particle images (no.)	106,020	73,170	61,066	47,438
Map resolution (Å)	2.70	3.21	3.20	3.38
FSC threshold	0.143	0.143	0.143	0.143
Refinement				
Initial model used (PDB code)	8Y69	8Y69	8Y69	4UFS
Model resolution (Å)	2.70	3.4	3.20	3.6
FSC threshold	0.143	0.143	0.143	0.143
Map sharpening *B* factor (Å^2)	-48.9	-85.2	-45.9	-83.5
Model composition				
Non-hydrogen atoms	8742	10742	10983	17577
Protein residues	1122	1381	1419	2255
Ligands	0	0	0	2
R.m.s. deviations				
Bond lengths (Å)	0.003	0.002	0.002	0.003
Bond angles (°)	0.526	0.491	0.515	0.661
Validation				
MolProbity score	1.88	2.04	2.06	2.26
Clashscore	6.93	7.35	6.68	8.55
Poor rotamers (%)	0.00	0.00	0.00	0.00
Ramachandran plot				
Favored (%)	94.46	94.17	94.79	94.36
Allowed (%)	5.54	5.76	5.14	5.55
Disallowed (%)	0.00	0.07	0.07	0.09

Supplementary Table. 2 | Oligonucleotide primers/gene fragments used in this study.

Primer	Sequence
pcDNA3.1-LGR4-forward	CTTGGTACCGAGCTCGGATCCGCCACCATGAAGAC CATCATCGCCCTGAGCTACAT
pcDNA3.1-LGR4-reverse	AACGGGCCCTCTAGACTCGACTTATCATCATCATCC TTGTAATCGCGGCCGCGTCTTTAACTCTTGGTAGAT
LGR4-F754A-forward	ATGTCGCTGCTCTAATCGCCACCAATTGCATCGCCT
LGR4-F754A-reverse	AGGCGATGCAATTGGTGGCGATTAGAGCAGCGACA T
LGR4-F765/766A-forward	TTCTGCCCTGTGGCGGCTGCTTCATTTGCACCATTG
LGR4-F765/766A-reverse	CAATGGTGCAAATGAAGCAGCCGCCACAGGGCAGA A
LGR4-F804A-F	CCAGTCCTGTATGTTTTCGCTAACCCAAAGTTTAAA GAA
LGR4-F804A-R	TTCTTTAAACTTTGGGTTAGCGAAAACATACAGGAC TGG
LGR4-Q742K-forward	CTCTCAGAAAACTCAAAATCTAGCATGATTAAGCA
LGR4-Q742K-reverse	TGCTTAATCATGCTAGATTTTGAGTTTTCTGAGAG
ZNRF3-H332A-F	CAGCACCACACCTGCCCCGCCTGTGCGCACAACAT CATA
ZNRF3-H332A-R	TATGATGTTGTGCGCACAGGCGGGGCAGGTGTGGT GCTG
ZNRF3RING-C311S/H313A-forward	AGGAGCTGCGGGTCATCCCCAGTACTGCCCGGTTTC ACAGGAAGTGCGTG
ZNRF3RING-C311S/H313A-reverse	CACGCACTTCCTGTGAAACCGGGCAGTACTGGGGA TGACCCGCAGCTCCT

Supplementary Table. 3 | FACS sequential gating in this study

	LGR4	First antibody	Second antibody
19-1	+ WT N-Flag	0.5μg/ml	1μg/ml
19-2	+ WT N-Flag	0.5μg/ml	1μg/ml
19-3	+ Q742K N-Flag	0.5μg/ml	1μg/ml
19-4	+ Q742K N-Flag	0.5μg/ml	1μg/ml
19-5	+ W751A N-Flag	0.5μg/ml	1μg/ml
19-6	+ W751A N-Flag	0.5μg/ml	1μg/ml
19-9	+ F804A N-Flag	0.5μg/ml	1μg/ml
19-10	+ F804A N-Flag	0.5μg/ml	1μg/ml
19-15	Empty vector	/	/